

Enhancement of superconducting critical temperature realized in La-Ce-H system at moderate pressures

Wuhao Chen,¹ Xiaoli Huang,^{1,*} Dmitrii V. Semenok,² Su Chen,¹ Kexin Zhang,¹ Artem R. Oganov² and Tian Cui,^{3,1,*}

¹ State Key Laboratory of Superhard Materials, College of Physics, Jilin University, Changchun 130012, China

² Skolkovo Institute of Science and Technology, Skolkovo Innovation Center, Bolshoy Boulevard 30, bldg. 1 Moscow, Russia 121205

³ School of Physical Science and Technology, Ningbo University, Ningbo 315211, China

*Corresponding authors' e-mails: huangxiaoli@jlu.edu.cn, cuitian@nbu.edu.cn

Abstract

Covalent and ionic superhydrides have become the two main camps in searching the high-temperature superconductors under pressure. They have been considered as important platforms for exploring ternary or multiple hydrides in order to further increase the T_c or decrease the stabilized pressure. In this work, we successfully synthesized the ternary hexagonal La-Ce polyhydrides by laser heating the La-Ce alloy (initial ratio: 2.5-3.5:1) in ammonia borane stable in the pressure range of 95-130 GPa. Superconductivity at around 176 K was strikingly preserved to ~ 100 GPa with a quite high figure of merit ($S=1.62$) among the synthesized hydrides. Additionally, the fitting of upper critical field at 0 K reached 216 T at 100 GPa. We also performed the contrast experiments and stabilized the binary high-temperature superconducting *hcp*-LaH₉₋₁₀ with $T_c\sim 103$ K at 78 GPa. In the pressure range of 95-130 GPa, the ternary hexagonal La-Ce-H system exhibits higher T_c than the binary La-H system with the maximum increment 100 K, both of which have been synthesized at the same high-pressure and high-temperature conditions. These results clearly indicate that the discovered La-Ce-H system not only enriches the high-temperature superconducting hydrides but also reconciles two high- T_c polyhydrides (*hcp*-LaH₉₋₁₀ and *hcp*-CeH₉) with high- T_c at moderate pressure.

Introduction

The recent discoveries of hydrogen based superconductors, H_3S [1-3], LaH_{10} [4-7], CeH_9 and CeH_{10} [8,9] and $C-S-H$ [10] as typical, have inspired enormous interests in multiple areas. Binary high temperature superconducting (HTSC) hydrides are basically divided into two categories: covalent and ionic. The theoretically [2] and experimentally [1] discovered earliest hydride H_3S belongs to the former. This type requires covalent bonding between hydrogen and light non-metal element gathering in the upper right corner of the periodic table. The latter are mainly from alkaline and rare earth metal elements with the character of high hydrogen content, called as polyhydrides or superhydrides. These sodalite-like clathrate structures containing hydrogen cages are leading the relevant research currently [11,12]. Besides, the layered hydrides with graphene-like hydrogen net are predicted to have great potential as high-temperature superconductors [13]. Although the superconducting records have been constantly refreshed, the acquisition of high-temperature superconducting phases at moderate pressures is still misty. Attentions have been turned to ternary hydrides. Sun et al. theoretically reported the ionic metal hydride Li_2MgH_{16} with the T_c reached 473 K at 250 GPa [14], indicating the huge possibility for HTSC in ternary system. The recent theoretical work proposed a series of ABH_8 type hydrides with HTSC, especially $LaBeH_8$ dynamically stable down to 20 GPa with a high $T_c \sim 185$ K. In contrast to theoretical studies, ternary hydrides have more research space in experiment, owing to the uncontrollable and complex synthesis.

Lanthanum superhydrides (La-H) [4-7,15-19] and cerium superhydrides (Ce-H) [8,9,20-23] have both been well studied before, and shared the same HTSC structures ($Fm-3m$ and $P6_3/mmc$). Importantly, lanthanum superhydrides have advantage in superconducting critical temperature, while the synthesis condition of cerium superhydrides are more favourable. As the lanthanide metals, La and Ce neighbor each other with very close atom radius and electronegativity. They can form continuous and homogenous solid solution. Thus, it is possible that using the La-Ce alloy as the initial reactant, we may get the ternary hydrides with similar structure to the binary La-H and Ce-H. A recent experimental work revealed that, even belonging to the different period, La and Y can be partly replaced by each other, and formed the HTSC hydrides with almost the same structure as their binary hydrides [24]. As is known to all, alloys may exhibit great difference and outstanding properties comparing with its compositions which can be adjusted by the relative content. Intra lanthanide alloys of Ce also show irregularities under pressure due to the *f* electron delocalization and have the tendency

to form mixed valent states already at ambient pressure. In the present work, we have synthesized the new HTSC La-Ce-H system, which stabilized in the pressure range of 95-130 GPa and possessed the same structure with La-H system. In the explored pressure range, the La-Ce-H system displayed the highest T_c comparing with binary La-H and Ce-H systems. Superconductivity in La-Ce-H system at around 176 K was strikingly preserved to ~ 100 GPa with a quite high figure of merit ($S=1.62$) among the synthesized metal hydrides below megabar pressure.

Results and Discussion

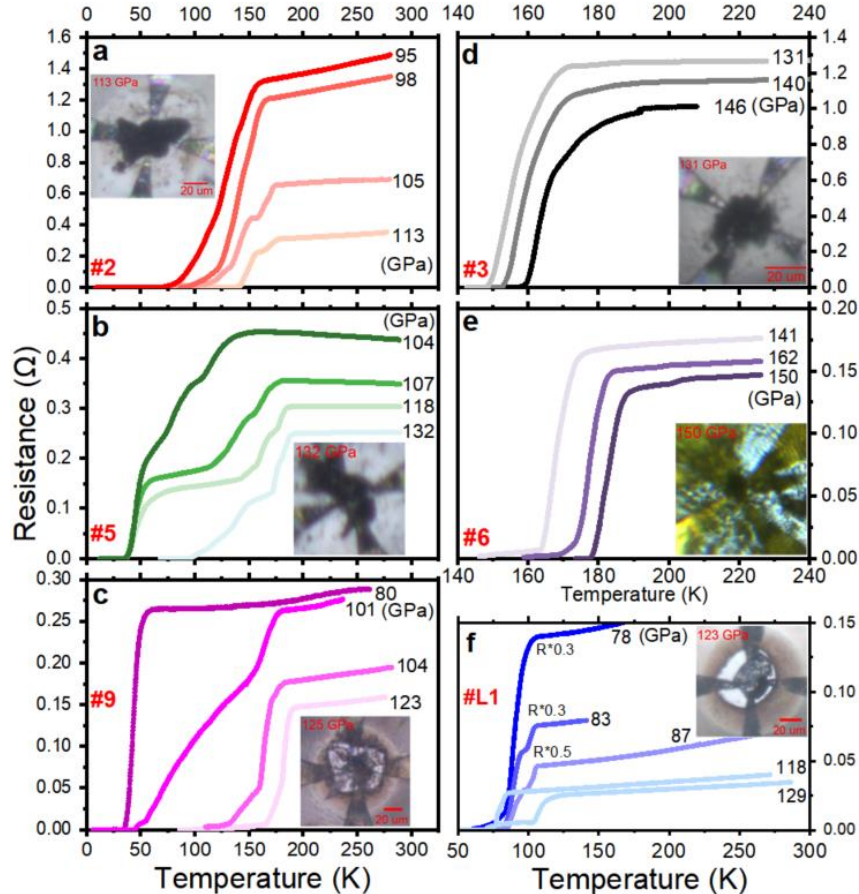


FIG. 1. Characterization of the superconducting transition by electrical resistance measurements at the selected pressures for the typical runs. Insets are the photographs of the sample chambers.

Electrical resistance measurements. Before loaded into the DAC, the prepared La-Ce alloys were characterized by SEM+EDX (Figs. S9,10,11, and 14), X-ray diffraction (XRD) (Fig. S2) and electrical measurements (Fig. S12,13), which indicate good homogeneity. The atomic ratio of La: Ce is between 2.5-3.5 for typical runs we discussed (Table S1), proved by EDX and XRD characterizations. The La-Ce alloys (run #1,2,3,7 and 8) without EDX characterization are supposed to have the content close to 3, since they were prepared in the similar condition (Fig. S1). After the synthesis of La-Ce-H

compounds by laser heating at specific pressures, we conducted the electrical measurements and plotted the typical results in Figure 1. In order to synthesize the high T_c phase at lower pressure, we heated cell #2 and #9 at initial 113 GPa and 120 GPa, respectively. Strikingly, T_{cs} at 177 K and 190 K were obtained for these two cells. Moreover, the T_{cs} s can be preserved to 155 K at 95 GPa (for cell #2) and 180 K at 104 GPa (for cell #9). To compare with the reported LaH_{10} , we laser heated cell #6 at 152 GPa, and the resistance started to drop from 187 K. T_c even decreased slightly with further compression to 156 GPa and 162 GPa subsequently, differ from the behavior of $C2/m$ LaH_{10} . Noteworthy, the pressure scale (P-diamond) used in this study gives a higher value than the scale of P-hydrogen by ~ 18 GPa [15]. Cell #3 and #5 were both laser-heated at around 130 GPa. However, T_c of cell #5 reached 188 K at 132 GPa, higher than T_c of cell #3 (170 K, 131 GPa), possibly due to the small difference of La content. Upon decreasing the pressure of cell #5 by 5 GPa, two apparent drops of resistance appeared. The higher T_c decreased gradually then and dropped to 132 K at 104 GPa. In contrast, the lower T_c (~ 37 K) is robust during decompression from 118 GPa (Fig. 1b) to at least 80 GPa (Fig. 1c).

To further confirm these high-temperature superconductivities, external magnetic field was applied to cell #2 to study the upper critical field (H_c) at 100 GPa (see Figure 2a). Fitting with WHH [25] (Werthamer-Helfand-Hohenberg) formula gives $H_c(0)$ of 216 T, the highest value reported in SC hydrides till now. The chaotic mixing of La and Ce atoms in ternary hydrides may introduce more defects which enhances the flux pinning, and increases the critical field. For cell #9, we applied the magnetic field, parallel and vertical to the culet, to study the possible anisotropy. Sample was kept exactly in the center of field in these two ways. This cell was measured in vertical position at 125 GPa first, which gave $H_c(0)=146$ T. After that, cell #9 was taken out of the cryostat and rotated 90 degrees. The pressure increased by 2 GPa, thus both the onset resistance and T_c decreased a little bit. However, $H_c(0)$ increased to 163 T in this situation (Fig.2b). In Figure 1c, further decompression of cell #9 from 123 GPa to 101 GPa repeated the tendency of high T_c phase in cell #2 and cell #5. It's worth noting that the transition width increases about 2.5 time from 104 GPa to 101 GPa. We think the high T_c phase maybe become instable below this pressure. All the cells show that the resistance of La-Ce-H sample increases a lot when pressure decreases.

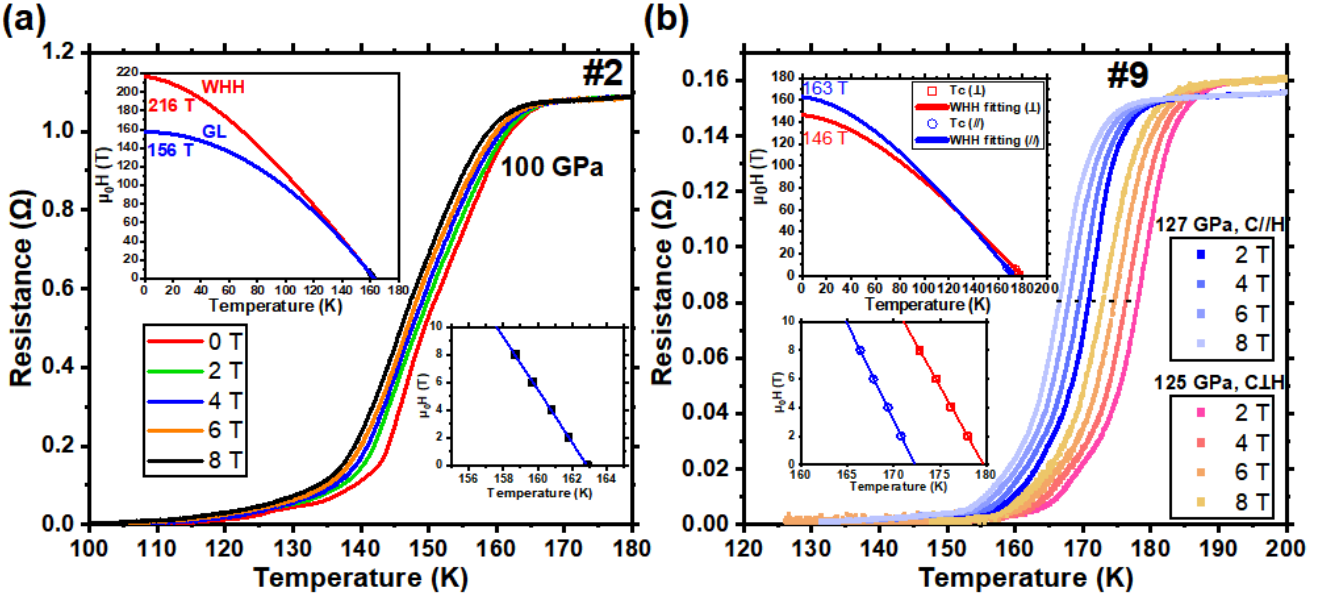


FIG. 2. Temperature dependences of electrical resistance at around superconducting transition in external magnetic fields. (a) Cell #2, Insets are the fitting with WHH formula and enlarged part of fitting. (b) Cell #9, C//H represents that the field is parallel to the culet, and C \perp H represents that the field is vertical to the culet. Insets are the fitting with WHH formula and enlarged part of fitting.

Comparing with our previous work on binary Ce-H system [8], we successfully synthesized the ternary La-Ce-H hydrides with higher critical temperature and upper magnetic field. However, no work reported the electrical measurements on binary La-H at pressure lower than 120 GPa currently. Thus, we performed the following research for comparison. For the La-H sample, an obvious resistance drop appeared at 84 K after first laser heating at 123 GPa, and the $H_c(0)$ is about 24.5 T (see Fig. S15 and Fig. S18). Compared with the obtained T_c of 190 K at 120 GPa in cell #9, T_c of La-H sample was lower than the one of La-Ce-H sample with about 100 K. Further increasing the pressure and laser-heating the cell #L1 (Fig. S15), another transition appeared with a higher T_c of 121 K at 129 GPa, and we thought that two SC phases were synthesized (Fig. S19). When decompressed the cell #L1, the ring cracks appeared on the bevel of diamond (Fig. S16 and Fig. S17). Luckily, the electrodes kept interconnected upon decompression to 78 GPa, and the sample still had the T_c at about 102 K (Fig. 1f), but then Pt electrodes broke.

Currently, there is no effective way to reduce the plastic deformation of the insulating gasket. Considering that the ring cracks was related to the cleavage feature and the anisotropy of hardness peculiar to single-crystal diamond (SCD), we noticed the nano-polycrystalline diamond (NPD) then. NPD is consisted of randomly oriented fine diamond crystals in nano scale and has higher Knoop hardness than SCD. Besides, NPD has been well studied for the ultrahigh-pressure generation and

high-pressure experimental measurements [40-45]. Here, we proposed the advantage of NPD used for the decompression process. Additionally, the longitudinal cleavage plane (Fig. S5) inside the SCD mainly because of the hydrogen diffusion can be effectively suppressed. Thus, we combined a flat NPD with 200 μm culet and a beveled SCD (200 μm to 100 μm in 8.5°) for run #L2 (Fig. S20). Pressure dropped from 113 GPa to 111 GPa after laser heating, and a very nice transition was detected at 80 K (Fig. S21). Upon further decompression, T_c can be tracked to 77 GPa with $T_c \sim 92$ K (Fig. S21 and S23).

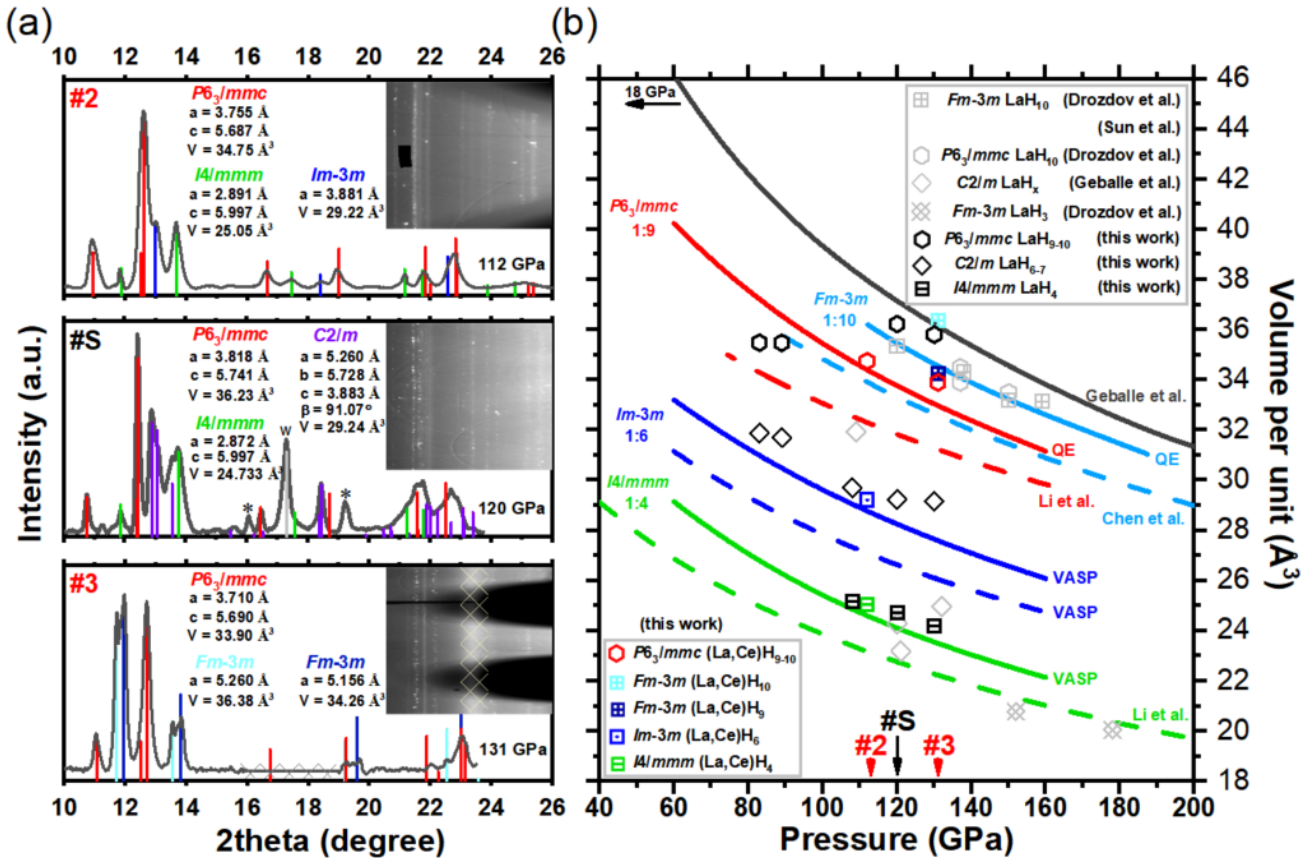


FIG. 3. Phase analysis of the compositions according to the synchrotron x-ray diffraction (0.6199 \AA) data. (a) XRD result and the related peaks indexing for La-Ce-H cells #2,3 and La-H cell #S. Insets are the integrated diffraction pattern. The diffraction of the impurity that locates on the seat surface of diamond is masked by gridlines (Fig. S7). (b) Unit cell volume of different phases as the dependence of pressure. Colorful and black symbols represent the result of our La-Ce-H and La-H work, respectively. The grey ones are taken from the references for La-H. Solid and dashed lines indicate the P - V relation of La-H and Ce-H, respectively.

XRD Analysis To reveal what real phases and structures determine the superconductivity, we have performed synchrotron XRD measurements on electrically characterized La-Ce-H (Fig. 3a, Fig. S4 and S6) and newly prepared La-H (Fig. S25) samples. Data were collected from three individual La-Ce-H electrical cells at different pressures, and from La-H cell #S during decompression. Result

shows the ubiquitous main phase with hexagonal symmetry from 82 GPa to 130 GPa for both samples. The superconducting $P6_3/mmc$ structure firstly comes to our consideration, since it has been well experimentally studied in CeH_9 and successfully synthesized in LaH_{10} . Noteworthy, only the symmetry of metal atoms can be experimentally determined by XRD, while hydrogen is undetectable, but the hydrogen content can be estimated according to the unit cell volume. We have plotted our P - V data together with the calculated or reported equation of state (EoS) of binary Ce-H and La-H for comparison (Fig. 3a). Firstly, all the EoS curves of CeH_x (dashed line) locates below LaH_x (solid line) for the same structure with equal hydrogen content which is related to the closer H-H distance in Ce-H system. The synthesized hcp -(La,Ce) H_x (black hexagon) shows smaller cell volume than hcp - LaH_x (red hexagon), but larger than hcp - CeH_9 , and they both have the hydrogen content between 9 and 10. The precise content cannot be determined, mainly because of the uncertainty in pseudo potential and pressure scale which has been reported in $Fm\text{-}3m$ LaH_{10} . Besides the hexagonal structure, two cubic polyhydrides were also discovered at 131 GPa in cell #3 (Fig.3b) which can be easily distinguished from binary $Fm\text{-}3m$ LaH_{10} according to the much lower T_c (Fig.1d). Geballe et al. laser-heated (2000 K) the mixture of La and pure hydrogen at similar pressure (120-130 GPa) before (Fig. S9 in Ref. [26]), while came to different results from ours that using the ammonia borane as the hydrogen source. The hydrogen content of their synthesized LaH_x is much lower (grey rhombus, Fig.3a). In addition, $I4/mmm$ (La,Ce) H_4 , $Im\text{-}3m$ (La,Ce) H_6 and $C2/m$ $\text{LaH}_{\sim 7}$ were also experimentally discovered in our work. The unexpected location of P - V data that even above the EoS of LaH_x can be partly explained with the overestimated pressure. The XRD also result gives the evidence that the La and Ce atoms take the form of randomly substitution in the ternary hexagonal La-Ce-H system, similar to the published La-Y-H [24] and La-Nd-H work [27].

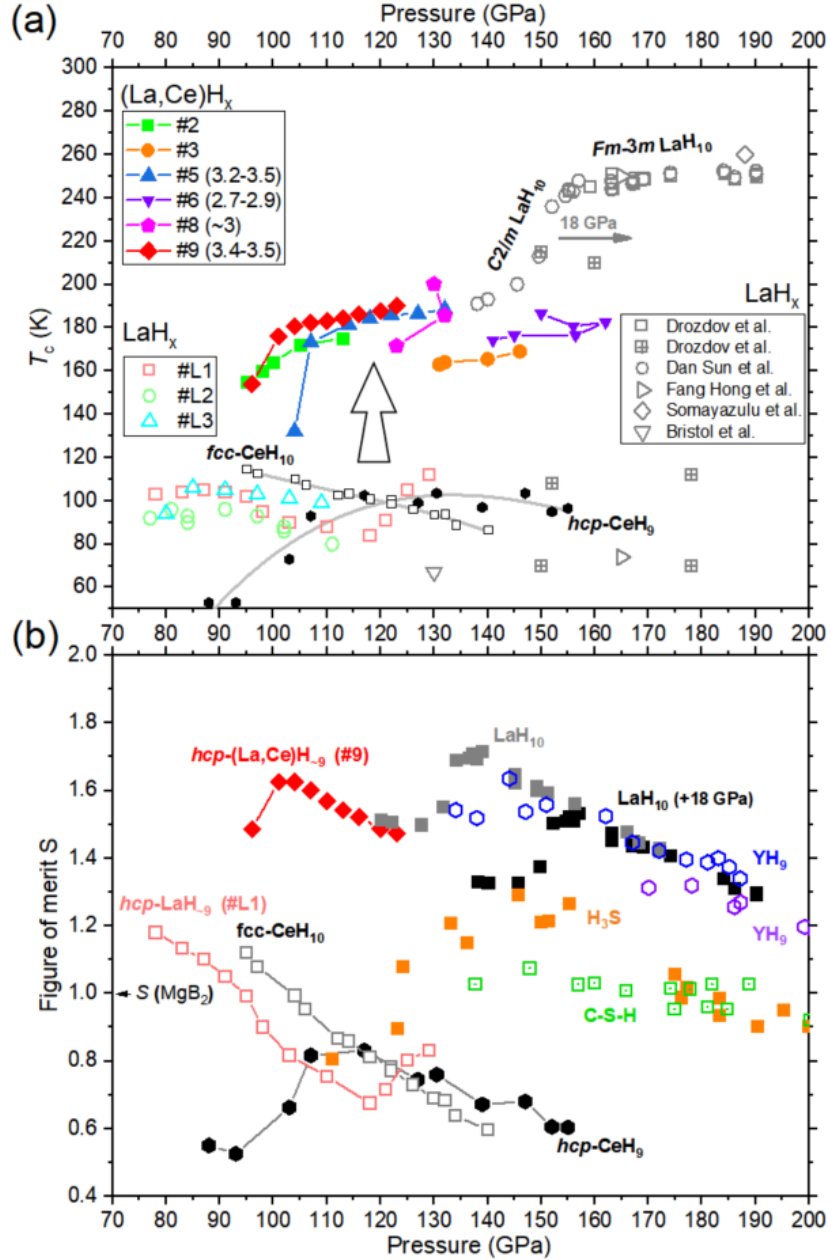


FIG. 4. The trend of superconducting critical temperature (T_c) and figure of merit (S) as a dependence of pressure for the hcp -(La,Ce)H₉₋₁₀, hcp -LaH₉₋₁₀ and some other typical superconducting hydrides. The data from Drozdov et al. and Dan Sun et al. that using the pressure scale of hydrogen vibration are artificially increased by 18 GPa to have a better comparison with our result. (a) the T_c - P relation among binary La-H, Ce-H and ternary La-Ce-H systems. (b) the S - P relation.

The T_c - P trend of binary La-H, Ce-H and the present synthesized ternary La-Ce-H systems are plotted together in Fig. 4a. T_{cs} of hcp -(La,Ce)H₉₋₁₀ decreases in about 0.59 K/GPa from 130 GPa to 105 GPa, with the maximum value of 200 K at 130 GPa for cell #8 (Fig. S13). We clarify here to exclude the possibility that transition comes from binary hydrides La-H or Ce-H system. Firstly, all the SEM+EDX, XRD and R - T measurements revealed good quality of La-Ce alloy at ambient

conditions. Especially, after just the compression of sample to certain pressure, electrical measurements showed sharp transitions to zero resistance at the temperature obviously lower than the T_c of pure La (Fig. S12 and S13). This indicates that the introduce of Ce atoms actually affects. Secondly, the superconducting transitions in La-Ce-H system are considered as arising from the main phase of $P6_3/mmc$ -(La,Ce)H₉₋₁₀, rather than $C2/m$ LaH₁₀. Meanwhile, laser heating the sample at 152 GPa didn't come to the T_c as high as LaH₁₀. Previously, Geballe et al. already detected the XRD evolution of $Fm-3m$ LaH₁₀ during decompression from 169 GPa to 27 GPa (Fig. S8 in Ref.[7]). We noticed that the main peak shifted to the higher angle abnormally at 121-109 GPa, and some new peaks arose. This is the characterization of decomposition and appearing of new phase, for example the $P6_3/mmc$ LaH₉₋₁₀. It is not accord with the near linearly T_c - P (0.6 K/GPa) trend of the current La-Ce-H system. Thirdly, T_{cs} of the synthesized La-Ce-H system are much larger than binary La-H and Ce-H system in the same pressure range. For comparison, the $P6_3/mmc$ -LaH₉₋₁₀ was synthesized at similar pressure with a much lower T_c (112 K, 129 GPa) which decreased to 84 K (118 GPa) first and then increased again. The figure of merit $S = \frac{T}{\sqrt{P^2 + T'^2}}$ [28] has been proposed to indicate the quality of the superconductors (T is the critical temperature, P is the related pressure and T' is the T_c of MgB₂ that equal to 39 K). As Fig. 4b shows, S of binary hcp -LaH₉₋₁₀ reached 1.18 (103 K, 78 GPa), comparable with $Fm-3m$ CeH₁₀ ($S=1.12$, 115 K and 95 GPa). Strikingly, the fusion of La and Ce (with initial ratio 2.5-3.5:1) led us to the discovery of ternary hcp -(La,Ce)H₉₋₁₀ with T_c reached 176 K at 101 GPa. It shows a quite high figure of merit $S=1.62$ among the experimentally reported superconducting hydrides. At last, we not only synthesized two SC-hydrides with S above 1, but also enhanced people's confidence to reach the next milestone like cuprates superconductors ($S = 3.5$ for HgBaCaCuO).

Conclusions

In this work, we have successfully synthesized the high temperature superconducting ternary La-Ce-H (La/Ce = 2.5~3.5) and binary La-H polyhydrides at pressures lower than 130 GPa, using the ammonia borane as the hydrogen source. Synchrotron XRD data revealed that these two hydrides both had the hexagonal structure with the hydrogen content reach 9-10 per unit cell. We detailedly studied their temperature dependence of electrical resistance in the decompression process. The hcp -(La,Ce)H₉₋₁₀ showed a relatively linearly T_c - P tendency with the rate about -0.6 K/ GPa from 130 GPa to 105 GPa. Strikingly, T_c was preserved to 176 K at about 100 GPa that came to a quite large figure

of merit ($S=1.62$) among the synthesized hydrides. Besides, the fitting of upper critical field $H_{c2}(0)$ reached the current highest 216 T at 100 GPa. T_c of *hcp*-LaH₉₋₁₀ is 112 K at 129 GPa which decreases first to 84 K at 118 GPa and then increase again to over 100 K at around 78 GPa. In the pressure range of 95-130 GPa, the ternary hexagonal La-Ce-H system exhibits higher T_c than the binary La-H system with the maximum increment 100 K, both of which have been synthesized at the same high-pressure and high-temperature conditions. Our work has evidenced the promising future in searching alloy-based high- T_c hydrides at ambient pressure.

Acknowledgments

The authors thank the staff of the Shanghai Synchrotron Radiation Facility for their help during the synchrotron XRD measurements. This work was supported by the National Key R&D Program of China (Grant No. 2018YFA0305900), the National Natural Science Foundation of China (Grants No. 52072188, No. 11974133, No. 51632002, and No. 51720105007), and the Program for Changjiang Scholars and Innovative Research Team in University (Grant No. IRT_15R23).

References

- [1] A. P. Drozdov, M. I. Eremets, I. A. Troyan, V. Ksenofontov, and S. I. Shylin, Conventional superconductivity at 203 kelvin at high pressures in the sulfur hydride system, *Nature* **525**, 73 (2015).
- [2] D. Duan, Y. Liu, F. Tian, D. Li, X. Huang, Z. Zhao, H. Yu, B. Liu, W. Tian, and T. Cui, Pressure-induced metallization of dense (H₂S)H₂ with high-T_c superconductivity, *Sci. Rep.* **4**, 6968 (2014).
- [3] Y. Li, J. Hao, H. Liu, Y. Li, and Y. Ma, The metallization and superconductivity of dense hydrogen sulfide, *The Journal of Chemical Physics* **140**, 174712 (2014).
- [4] H. Y. Liu, I. I. Naumov, R. Hoffmann, N. W. Ashcroft, and R. J. Hemley, Potential high-T_c superconducting lanthanum and yttrium hydrides at high pressure, *Proc. Natl. Acad. Sci. U. S. A.* **114**, 6990 (2017).
- [5] A. P. Drozdov, P. P. Kong, V. S. Minkov, S. P. Besedin, M. A. Kuzovnikov, S. Mozaffari, L. Balicas, F. F. Balakirev, D. E. Graf, V. B. Prakapenka, E. Greenberg, D. A. Knyazev, M. Tkacz, and M. I. Eremets, Superconductivity at 250 K in lanthanum hydride under high pressures, *Nature* **569**, 528 (2019).
- [6] M. Somayazulu, M. Ahart, A. K. Mishra, Z. M. Geballe, M. Baldini, Y. Meng, V. V. Struzhkin, and R. J. Hemley, Evidence for Superconductivity above 260 K in Lanthanum Superhydride at Megabar Pressures, *Phys. Rev. Lett.* **122**, 027001 (2019).
- [7] Z. M. Geballe, H. Y. Liu, A. K. Mishra, M. Ahart, M. Somayazulu, Y. Meng, M. Baldini, and R. J. Hemley, Synthesis and Stability of Lanthanum Superhydrides, *Angew. Chem. Int. Ed.* **57**, 688 (2018).
- [8] W. Chen, D. V. Semenok, X. Huang, H. Shu, X. Li, D. Duan, T. Cui, and A. R. Oganov, High-Temperature Superconducting Phases in Cerium Superhydride with a T_c up to 115 K below a Pressure of 1 Megabar, *Phys. Rev. Lett.* **127** (2021).
- [9] X. Li, X. L. Huang, D. F. Duan, C. J. Pickard, D. Zhou, H. Xie, Q. Zhuang, Y. P. Huang, Q. Zhou, B. B. Liu, and T. Cui, Polyhydride CeH₉ with an atomic-like hydrogen clathrate structure, *Nat. Commun.* **10**, 3461 (2019).
- [10] E. Snider, N. Dasenbrock-Gammon, R. McBride, M. Debessai, H. Vindana, K. Vencatasamy, K. V. Lawler, A. Salamat, and R. P. Dias, Room-temperature superconductivity in a carbonaceous sulfur hydride, *Nature* **586**, 373

(2020).

[11] H. Wang, J. S. Tse, K. Tanaka, T. Iitaka, and Y. M. Ma, Superconductive sodalite-like clathrate calcium hydride at high pressures, *Proc. Natl. Acad. Sci. U. S. A.* **109**, 6463 (2012).

[12] L. Ma, K. Wang, Y. Xie, X. Yang, Y. Wang, M. Zhou, H. Liu, G. Liu, H. Wang, and Y. Ma, Experimental observation of superconductivity at 215 K in calcium superhydride under high pressures, *arXiv pre-print server* (2021).

[13] H. Xie, Y. Yao, X. Feng, D. Duan, H. Song, Z. Zhang, S. Jiang, S. A. T. Redfern, V. Z. Kresin, C. J. Pickard, and T. Cui, Hydrogen Pentagraphenelike Structure Stabilized by Hafnium: A High-Temperature Conventional Superconductor, *Phys. Rev. Lett.* **125** (2020).

[14] Y. Sun, J. Lv, Y. Xie, H. Liu, and Y. Ma, Route to a Superconducting Phase above Room Temperature in Electron-Doped Hydride Compounds under High Pressure, *Phys. Rev. Lett.* **123**, 097001 (2019).

[15] D. Sun, V. S. Minkov, S. Mozaffari, Y. Sun, Y. Ma, S. Chariton, V. B. Prakapenka, M. I. Eremets, L. Balicas, and F. F. Balakirev, High-temperature superconductivity on the verge of a structural instability in lanthanum superhydride, *Nat. Commun.* **12** (2021).

[16] I. Errea, F. Belli, L. Monacelli, A. Sanna, T. Koretsune, T. Tadano, R. Bianco, M. Calandra, R. Arita, F. Mauri, and J. A. Flores-Livas, Quantum crystal structure in the 250-kelvin superconducting lanthanum hydride, *Nature* **578**, 66 (2020).

[17] F. Hong, L. Yang, P. Shan, P. Yang, Z. Liu, J. Sun, Y. Yin, X. Yu, J. Cheng, and Z. Zhao, Superconductivity of Lanthanum Superhydride Investigated Using the Standard Four-Probe Configuration under High Pressures, *Chin. Phys. Lett.* **37**, 107401 (2020).

[18] V. Struzhkin, B. Li, C. Ji, X.-J. Chen, V. Prakapenka, E. Greenberg, I. Troyan, A. Gavriliuk, and H.-k. Mao, Superconductivity in La and Y hydrides: Remaining questions to experiment and theory, *Matter and Radiation at Extremes* **5**, 028201 (2020).

[19] L. Y. Fang Hong, Pengfei Shan, Pengtao Yang, Ziyi Liu, Jianping Sun, Yunyu Yin, Xiaohui Yu, Jinguang Cheng, and Z. Zhao, Superconductivity of Lanthanum Superhydride Investigated Using the Standard Four-Probe Configuration under High Pressures, *Chin. Phys. Lett.*, 107401%V 37 (2020).

[20] N. P. Salke, M. M. Davari Esfahani, Y. Zhang, I. A. Kruglov, J. Zhou, Y. Wang, E. Greenberg, V. B. Prakapenka, J. Liu, A. R. Oganov, and J.-F. Lin, Synthesis of clathrate cerium superhydride CeH9 at 80-100 GPa with atomic hydrogen sublattice, *Nat. Commun.* **10**, 4453 (2019).

[21] H. Jeon, C. Wang, S. Yi, and J.-H. Cho, Origin of enhanced chemical precompression in cerium hydride CeH9, *Sci. Rep.* **10**, 16878 (2020).

[22] B. Li, Z. Miao, L. Ti, S. Liu, J. Chen, Z. Shi, and E. Gregoryanz, Predicted high-temperature superconductivity in cerium hydrides at high pressures, *J. Appl. Phys.* **126**, 235901 (2019).

[23] F. Peng, Y. Sun, C. J. Pickard, R. J. Needs, Q. Wu, and Y. M. Ma, Hydrogen Clathrate Structures in Rare Earth Hydrides at High Pressures: Possible Route to Room-Temperature Superconductivity, *Phys. Rev. Lett.* **119**, 107001 (2017).

[24] D. V. Semenok, I. A. Troyan, A. G. Ivanova, A. G. Kvashnin, I. A. Kruglov, M. Hanfland, A. V. Sadakov, O. A. Sobolevskiy, K. S. Pervakov, I. S. Lyubutin, K. V. Glazyrin, N. Giordano, D. N. Karimov, A. L. Vasiliev, R. Akashi, V. M. Pudalov, and A. R. Oganov, Superconductivity at 253 K in lanthanum–yttrium ternary hydrides, *Mater. Today* **48**, 18 (2021).

[25] N. R. Werthamer, E. Helfand, and P. C. Hohenberg, Temperature and Purity Dependence of the Superconducting Critical Field, Hc2. III. Electron Spin and Spin-Orbit Effects, *Physical Review* **147**, 295 (1966).

[26] F. v. Rohr, M. J. Winiarski, J. Tao, T. Klimczuk, and R. J. Cava, Effect of electron count and chemical complexity in the Ta-Nb-Hf-Zr-Ti high-entropy alloy superconductor, *Proceedings of the National Academy of Sciences* **113**,

E7144 (2016).

[27] V. S. Dmitrii, A. T. Ivan, V. S. Andrey, Z. Di, G. Michele, G. K. Alexander, A. K. Ivan, A. B. Alexey, Y. T. e. Konstantin, V. C. Alexander, A. S. Oleg, S. P. Kirill, S. Alexey Yu, H. Toni, F. Tobias, D. G. Audrey, W. T. Stanley, N. Yuki, S. Katsuya, M. P. Vladimir, S. L. Igor, and R. O. Artem, Research Square (2022).

[28] C. J. Pickard, I. Errea, and M. I. Eremets, Superconducting Hydrides Under Pressure, *Annu. Rev. Condens. Matter Phys.* **11**, 57 (2020).

Supplemental Information

Wuhao Chen,¹ Xiaoli Huang,^{1,*} Dmitrii V. Semenok,² Su Chen,¹ Kexin Zhang,¹ Artem R. Oganov² and Tian Cui,^{3,1,*}

¹ State Key Laboratory of Superhard Materials, College of Physics, Jilin University, Changchun 130012, China

² Skolkovo Institute of Science and Technology, Skolkovo Innovation Center, Bolshoy Boulevard 30, bldg. 1 Moscow, Russia 121205

³ School of Physical Science and Technology, Ningbo University, Ningbo 315211, China

*Corresponding authors' e-mails: huangxiaoli@jlu.edu.cn, cuitian@nbu.edu.cn

Experimental details

The La-Ce alloys were prepared by the multitarget magnetron sputtering (Fig.S_). We sputtered the La (99.9%) and Ce (99.9%) metals simultaneously to the glass slide using DC and RF power supplies, respectively. The Ar pressure is 1.5 Pa, and both targets were pre-sputtered to remove the surface oxides. Depend on the distance to target, the La:Ce ratio has certain distribution. The LaCe alloy was further characterized by scanning electron microscope (SEM, Regulus 8100), equipped with energy dispersive x-ray spectroscopy (EDS). The La-Ce samples on the glass side for high pressure experiment were located very close to the SEM characterized area while kept strictly in the glove box ($O_2 < 0.01$ ppm, $H_2O < 0.01$ ppm). Normal type-Ia diamonds with 60-150 μ m culets single beveled to 250-300 μ m were used, and pressure was measured according to the Raman vibration edge of diamond using the Akahama's calibration[1,2]. The resistance was measured by four-probe method using the delta model of Keithley current source (Model 6221, 1 mA) and voltmeter (Model 2182A). The electrodes were integrated to the diamond by lithographic Mo (300-500 nm thick)[3] or manual cutting Pt (2-3 μ m thick) foil. To protect the electrodes during decompression, we tested the nano-polycrystalline diamonds (NPD) without bevels in some runs. Due to the high fluorescence background of NPDs, their Raman edge cannot be distinguished. Thus, the NPDs (200-300 μ m culet) were combined with the normal diamonds, and the electrodes were set in the NPD side. The indentation of tungsten gasket was insulated by c-BN/epoxy first, and the bevel part was filled with oxides (Al_2O_3 , MgO)/epoxy. The La-Ce sample was loaded into the chamber filled with ammonia borane (AB) which acts as the hydrogen source. Sample was heated at target pressure by the 1070 nm infrared laser with 3-5 μ m focus point and 1-3 s exposure time. After that, we inserted the cells into the helium cryostat (1.5-300 K) equipped with 0-9 T superconducting magnet for low temperature electrical

measurements. Crystal structure was characterized by the synchrotron X-ray diffraction on the BL15U1 synchrotron beamline at the Shanghai Synchrotron Research Facility (SSRF) with 0.6199 Å wavelength. The experimental XRD images were integrated and analyzed using the Dioptas software package for possible phases[4]. To fit the diffraction patterns and get the cell parameter, we analyzed the data using Materials Studio and Jana2006 programs[5] with the Le Bail method[6].

Run	Initial Sample	La:Ce	Laser heating pressure
#1	(La, Ce) +AB	Unknown	102 GPa- 82 GPa
#2	(La, Ce) +AB	Unknown	113 GPa-112 GPa
#3	(La, Ce) +AB	Unknown	130 GPa-131 GPa
#4	(La, Ce) +AB	≈6	107 GPa-103 GPa
#5	(La, Ce) +AB	3. 2-3. 5	129 GPa-132 GPa
#6	(La, Ce) +AB	2. 7-2. 9	152 GPa-150 GPa
#7	(La, Ce) +AB	Unknown	without LH
#8	(La, Ce) +AB	Unknown	129 GPa-131 GPa, 131 GPa-130 GPa
#9	(La, Ce) +AB	3. 4-3. 5	120 GPa-118 GPa, 122 GPa-120 GPa, 127 GPa-125 GPa
#L1	La+AB	pure La	125 GPa-123 GPa, 130 GPa-127 GPa, 132 GPa- 129 GPa
#L2	La+AB	pure La	113 GPa-111 GPa
#L3	La+AB	pure La	109 GPa heated
#S	La+AB	pure La	132 GPa-130 GPa

Table S1. Information about the initial sample and the pressure before and after laser heating for all the experimental runs.

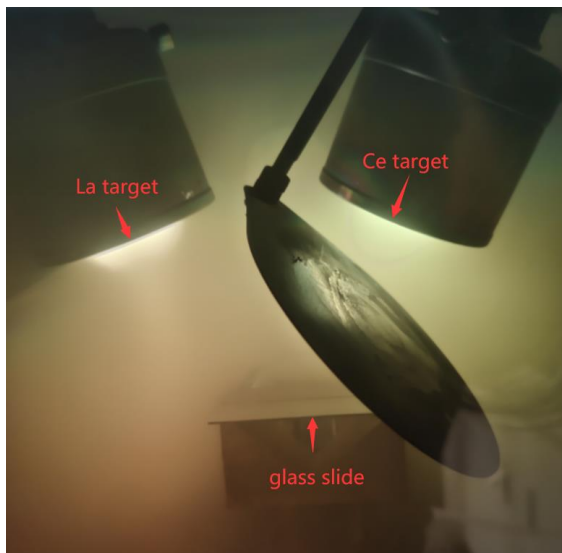


Fig. S1. Photograph of the chamber inside the magnetron sputtering equipment. La and Ce ions mixed with each other in the Ar atmosphere and then deposited on the glass slide.

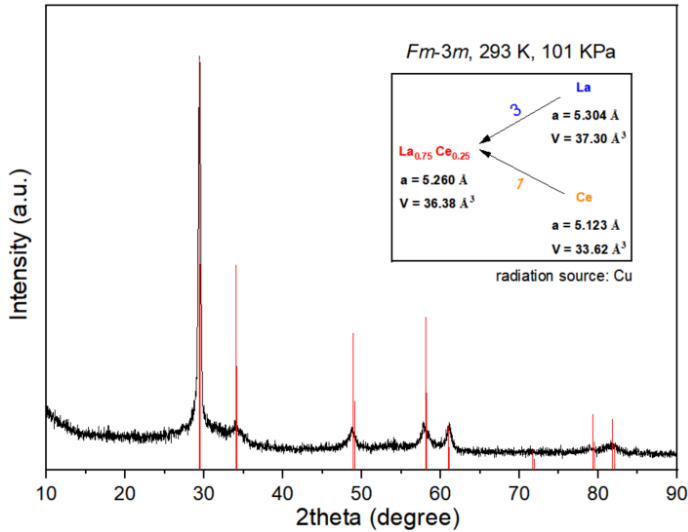


Fig. S2. XRD (Cu: $K_{\alpha 1}=1.54056\text{\AA}$, $K_{\alpha 2}=1.54439\text{\AA}$) of the La-Ce alloy at ambient conditon. Red lines are the indexing with calcualted diffraction of *Fm-3m* structure. Inset contains the related cell parameters.

Run #1

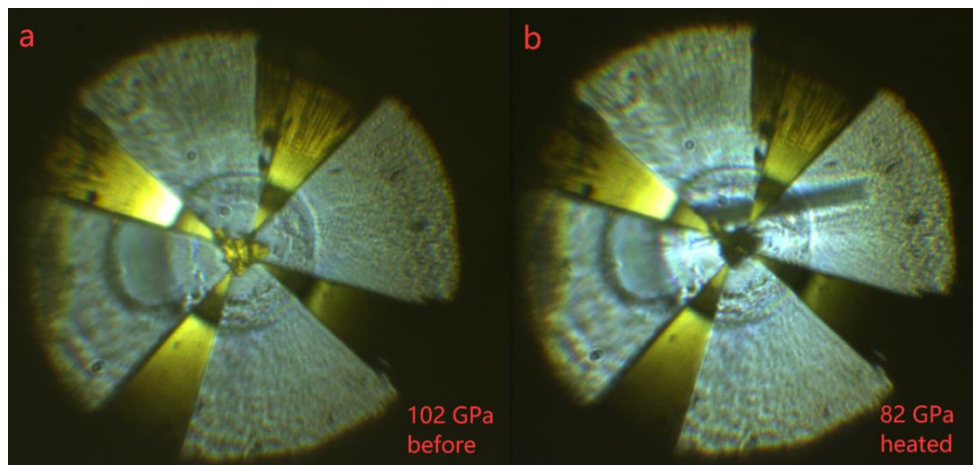


Fig. S3. Photographs of cell #1 before (a) and after (b) laser heating. Vertical crack appeared and grew gradually during laser heating.

Run #2

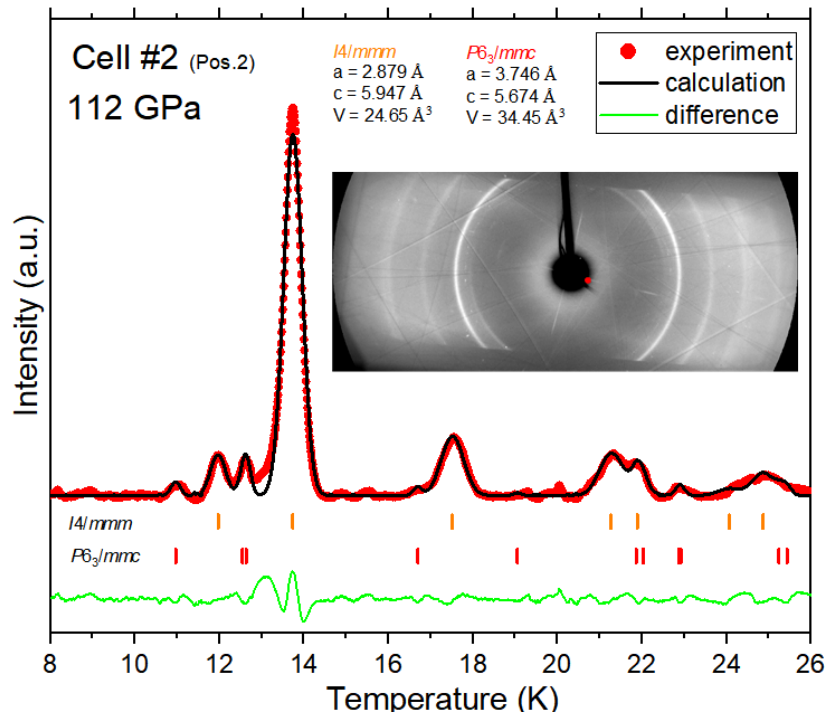


Fig. S4. Le Bail fitting of the XRD for another detected sample position of cell #2 at 112 GPa. Inset is the diffraction pattern.

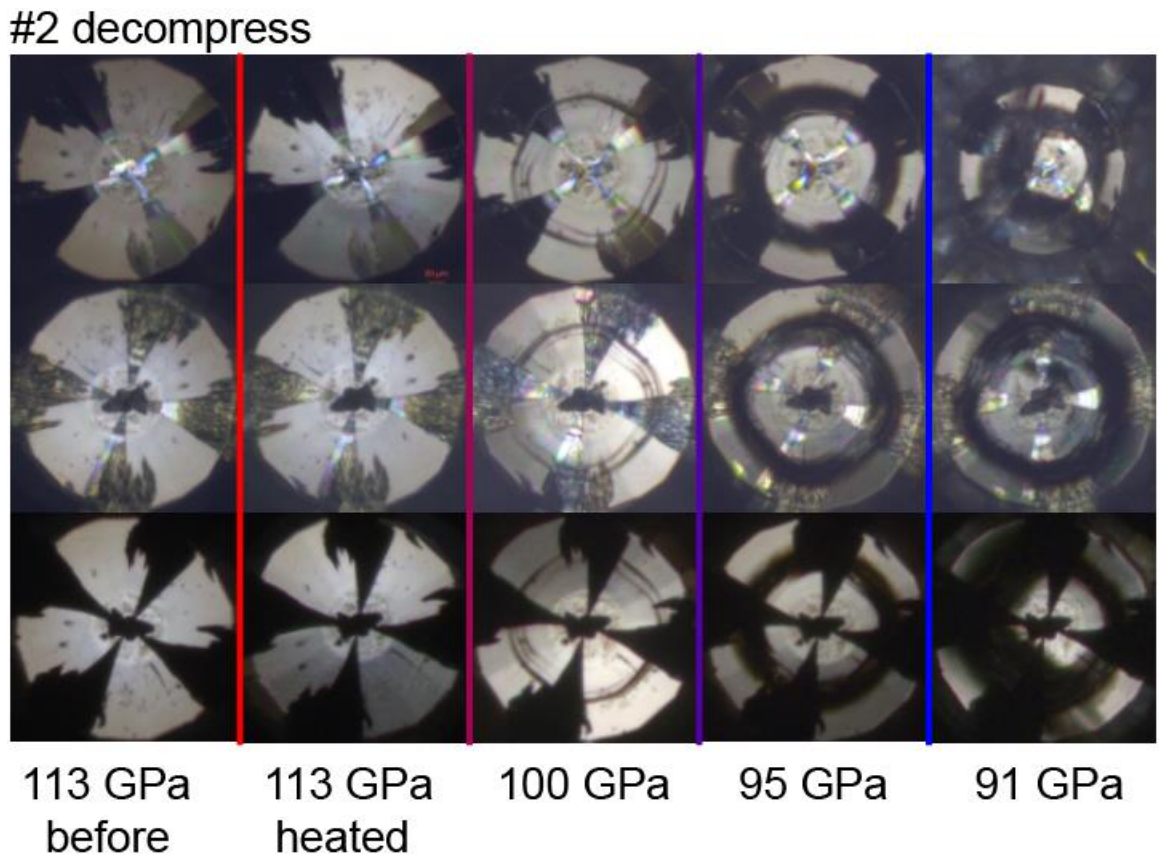


Fig. S5 Behavior of the diamond's bevel during decompression of cell #2 from different photographic views.

Run #3

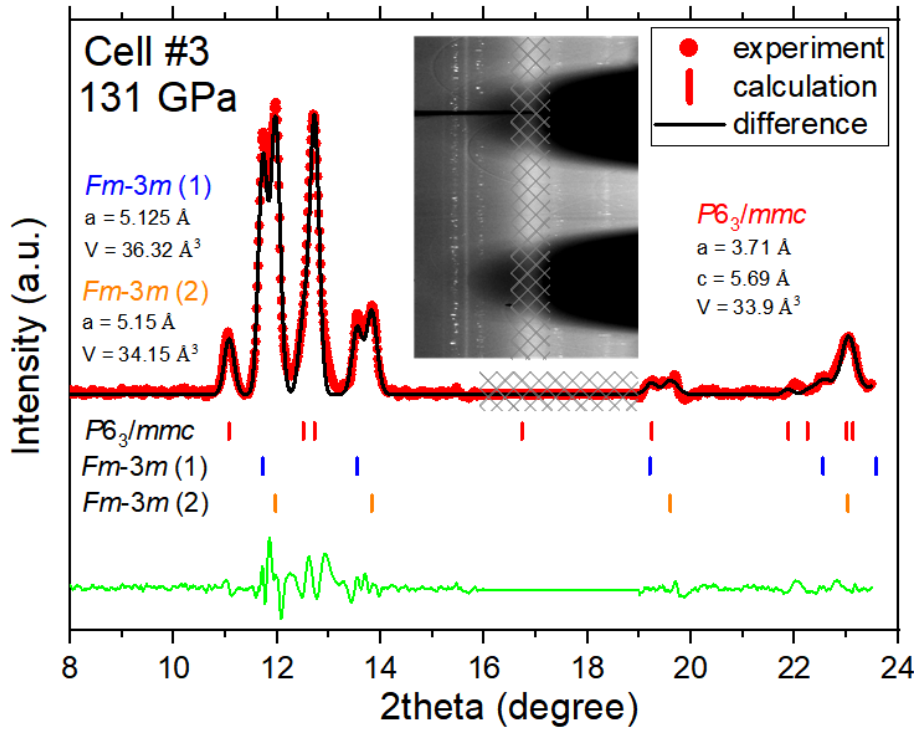


Fig. S6. Le Bail fitting of the XRD for cell #3 at 131 GPa. Inset is the integrated diffraction pattern. The diffraction of the impurity that locates on the seat surface of diamond as discussed below is masked by gridlines.

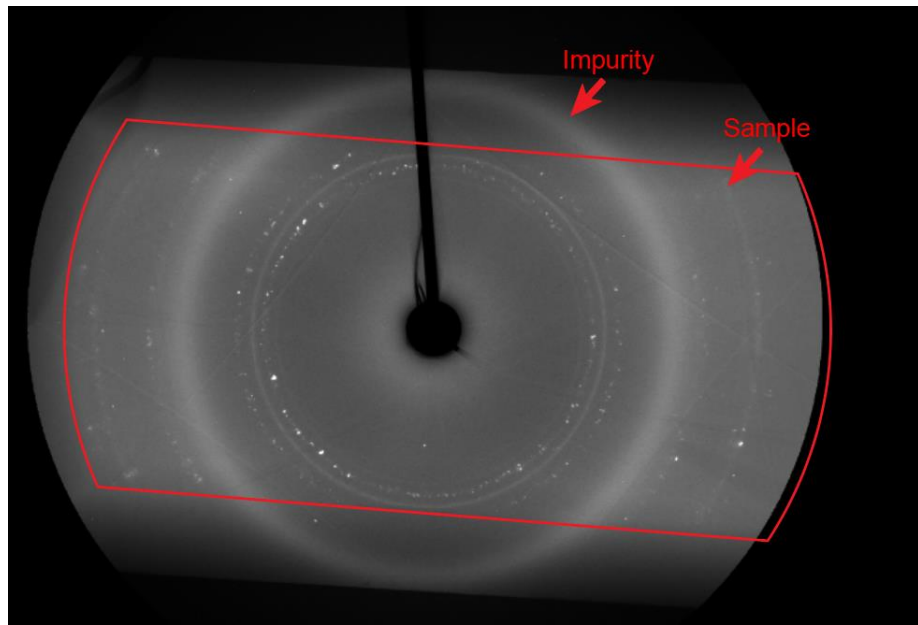


Fig. S7. XRD diffraction pattern of cell #3 at 131 GPa. The red frame represents the projection of the long opening in diamond seat. The sample shows a set of incomplete diffraction circles because of the occlusion of seat, while the impurity shows a broad entire circle. This means the impurity is not in the sample chamber while closer to the diamond seat. It could be something dirty on the seat surface of diamond.

Run #4

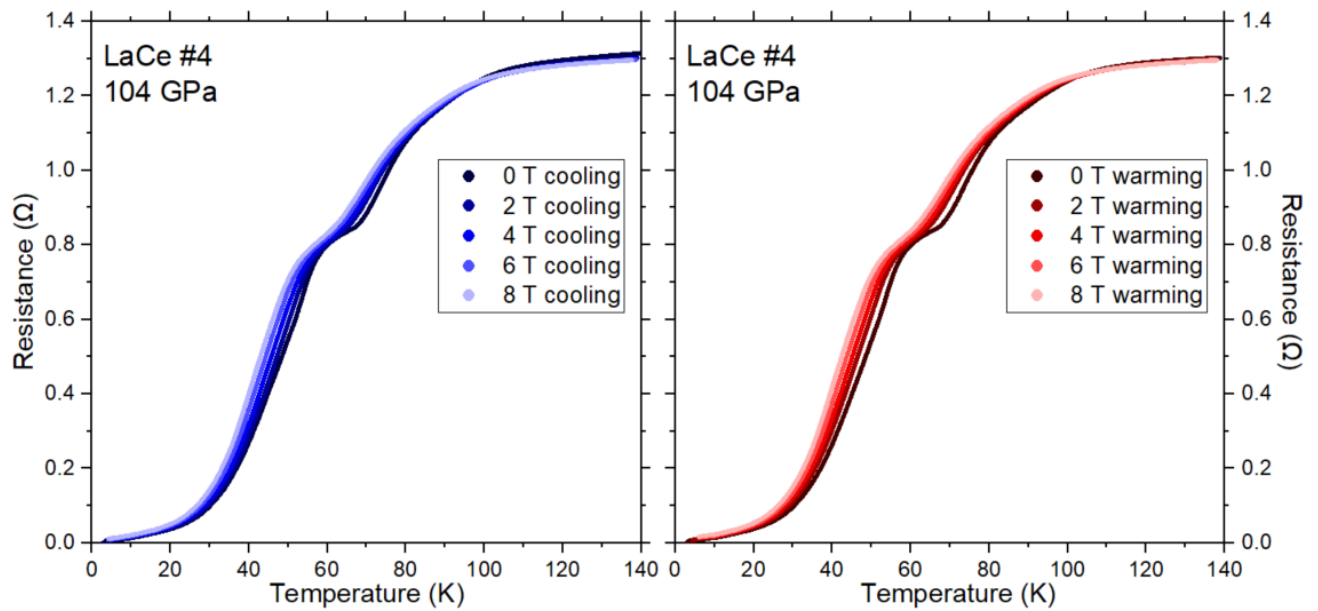


Fig. S8. Temperature dependence of the resistance of run #4 at superconducting transition in external magnetic field for cooling(left) and warming(right) cycle. Experimental sequence: cooling and measuring R - T in 0 T, warming and measuring R - T in 0 T, increasing the field to 2 T, cooling and measuring R - T in 2 T...

Run #5

#5 pos.1

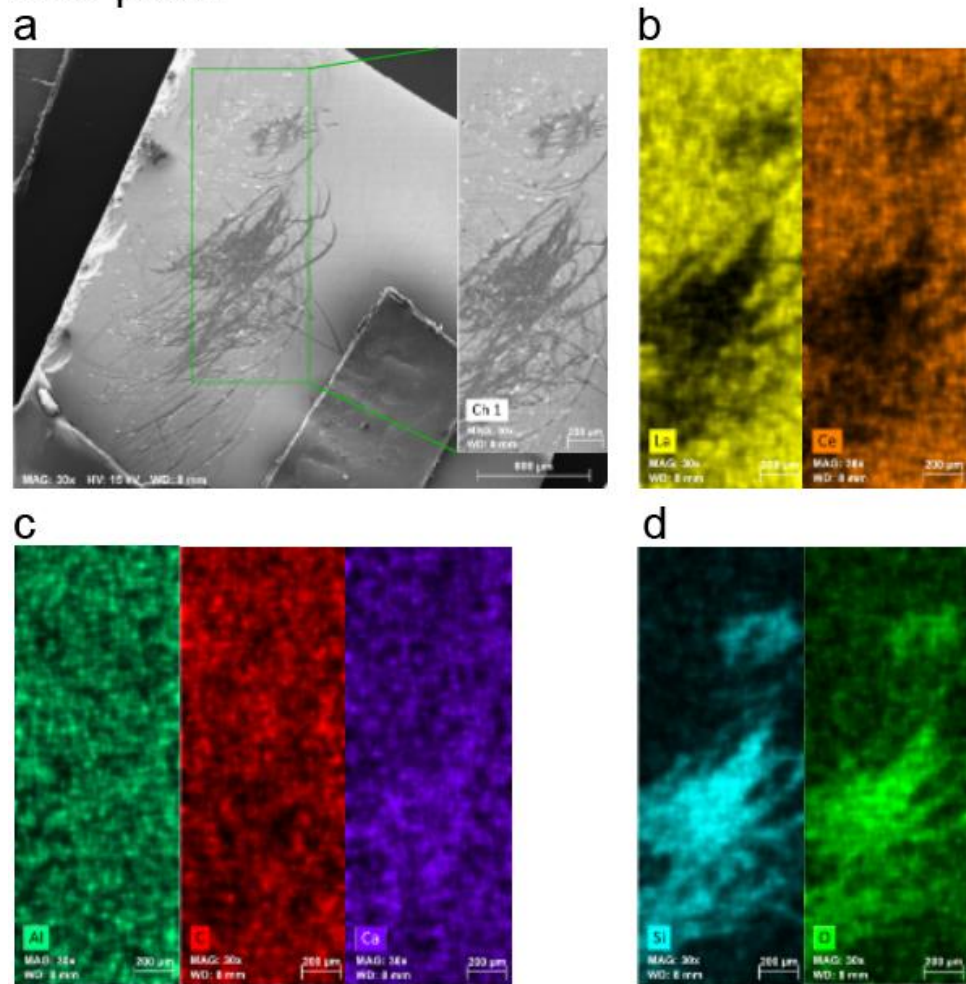


Fig. S9. Scanning electron microscope (SEM) and energy dispersive X-ray spectroscopy (EDX) analysis of La-Ce alloy in run #5, pos. 1 (a) The SEM photo of the sample on glass slide. (b), (c), (d) The elements distribution in the area of green rectangle

In run #5, the alloy composition was characterized after sample loading. We use the tungsten needle to scratch the La-Ce layer on the glass slide to get particles, thus there were traces left (Fig. S a). As we can see in Fig. S b, La and Ce were both uniformly distributed except on the scratched area. The Si and O mainly come from the glass slide since the scratched area has high intensity (Fig. S d). On the La-Ce surface, there was a tiny oxygen element which was because of the formed oxides during transfer. Moreover, Al, C, Ca exist all over the selected region. Hence, it can be viewed as the background signal. Fig. S shows that the scratched particles have uniform distribution of La and Ce. The sputtered La-Ce can form clusters or smooth solid solution.

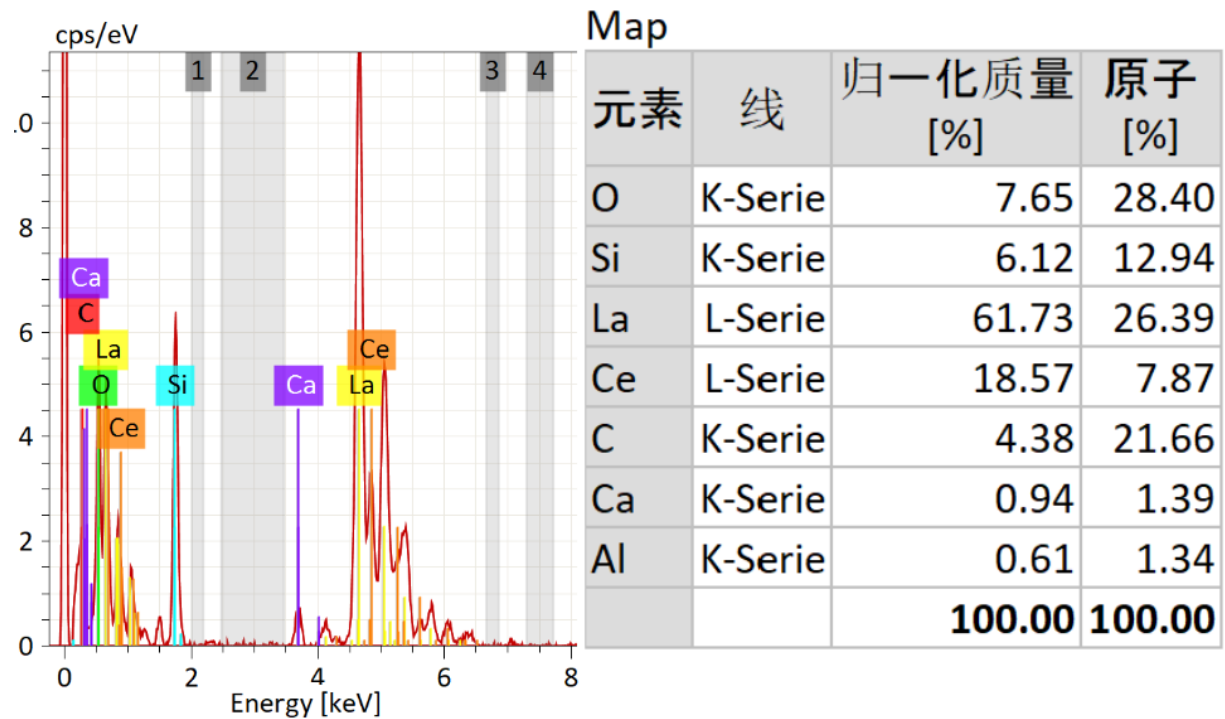


Fig. S10. Elements content analysis by EDX in run #5.

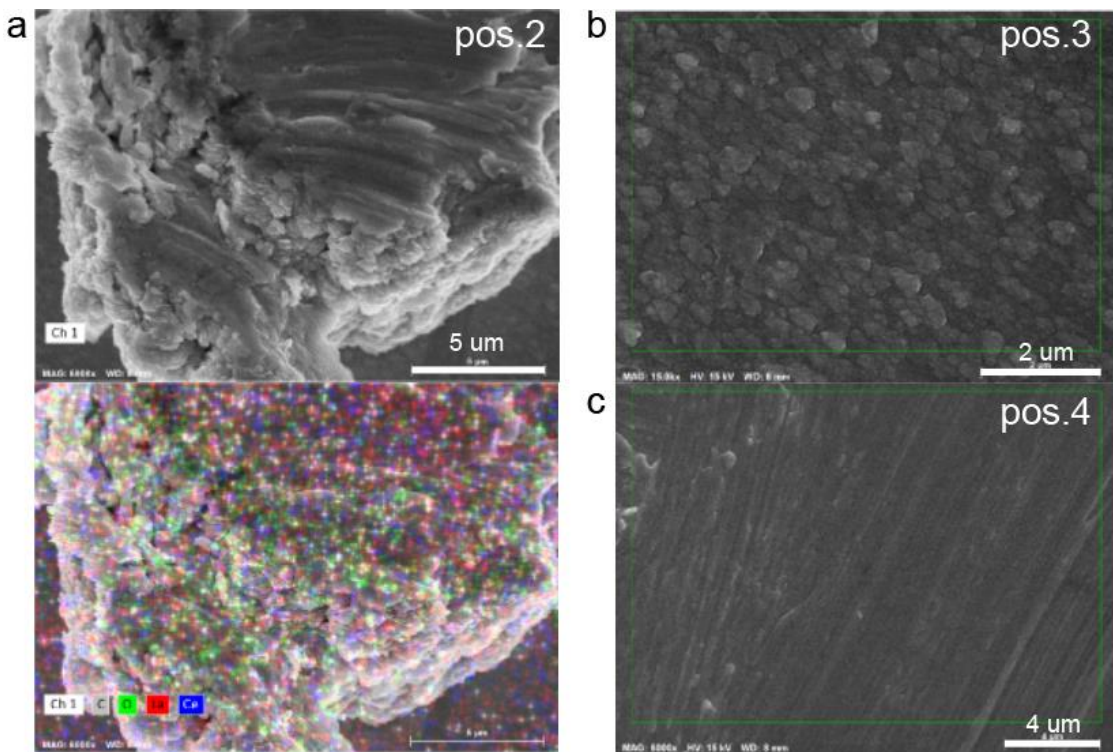


Fig. S11. The SEM photos of other positions in run #5. (a) Upper: the photo of the selected particle Below: Element distribution on the particle. (b) and (c) are positions 3 and 4.

Run #7

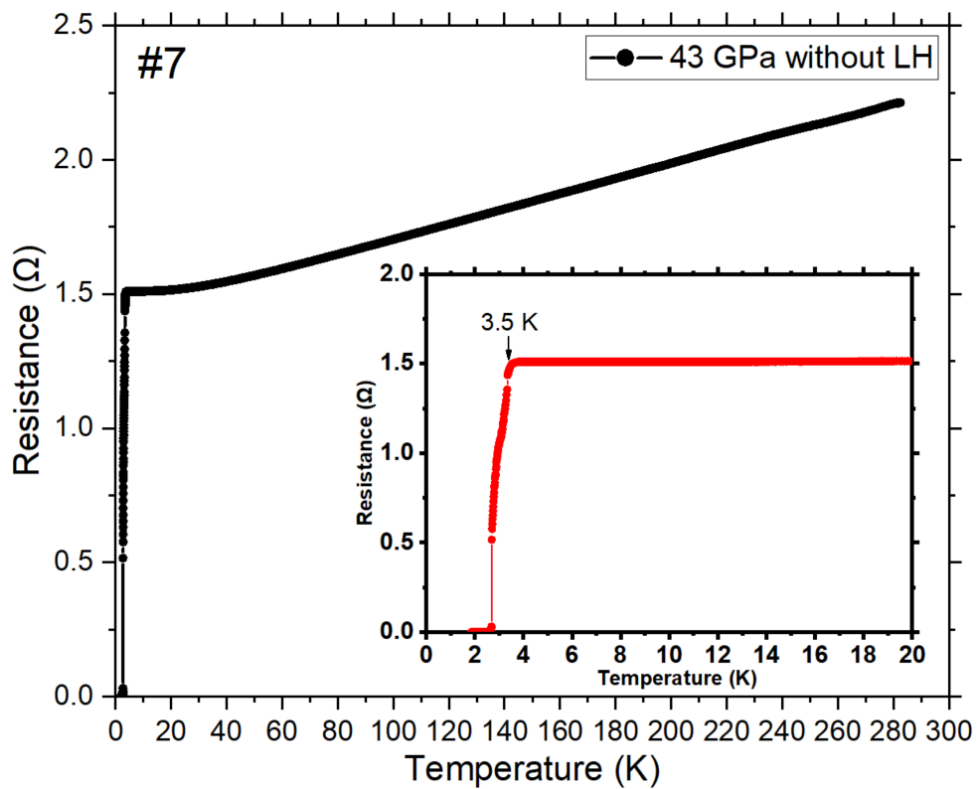


Fig. S12. The R - T data of La-Ce alloy in run #7 at 43 GPa without laser heating (LH). Inset is the enlarged part.

Run #8

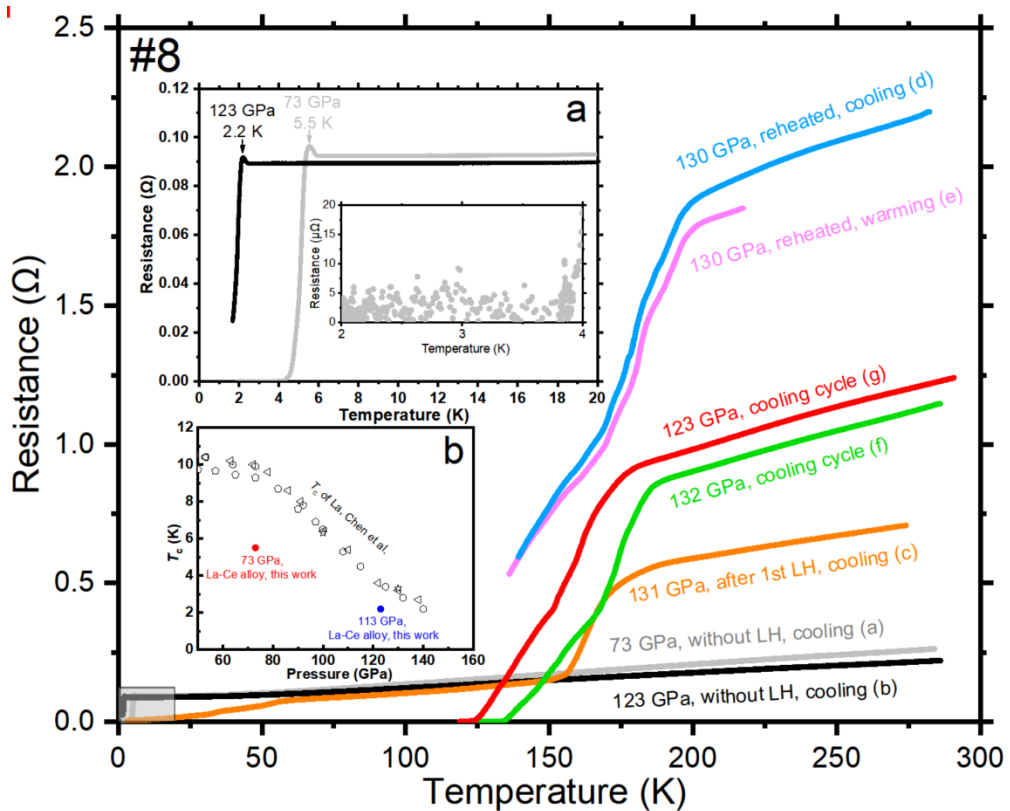


Fig. S13. R - T data of run #8. Letters from *a* to *f* indicate the order of experiments. Inset (a) is the enlarged part

of superconducting transition of La-Ce alloy before laser heating. Inset (b) is the comparison of T_c between La-Ce alloy and pure La.

Run #9

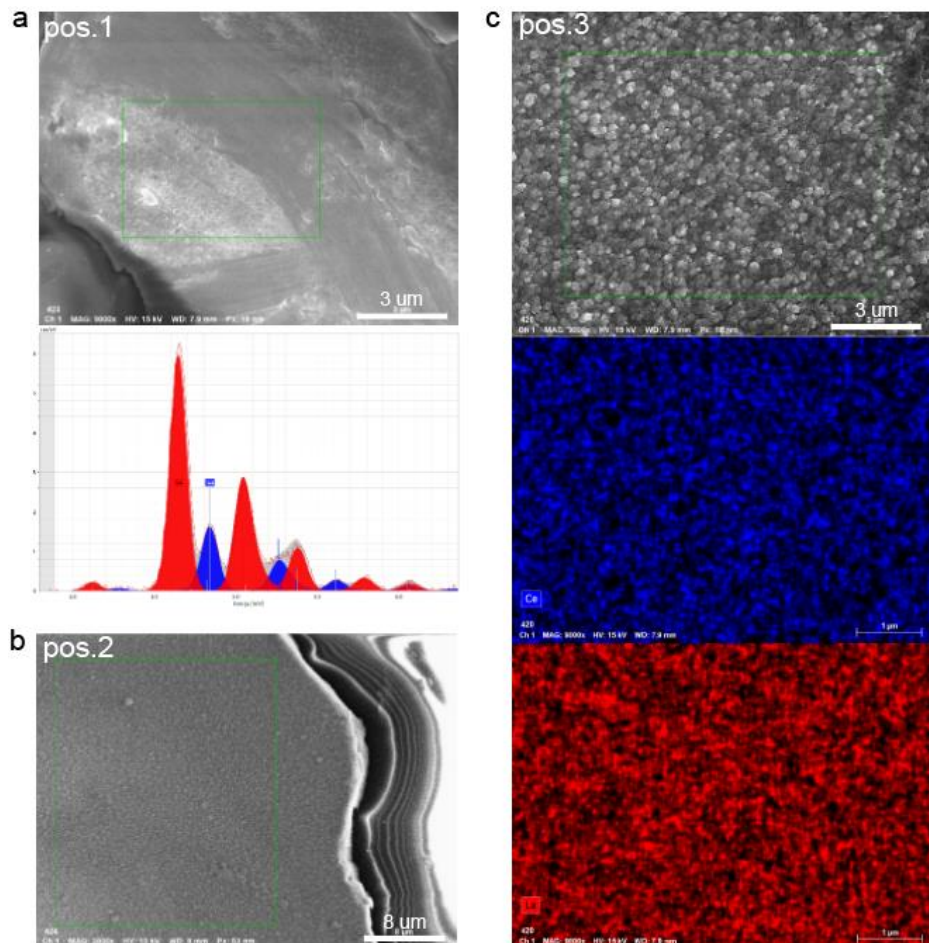


Fig. S14. The EDX analysis of La-Ce alloy in run #9. (a) Upper: the photo of the selected particle Below: L-Serie energy spectrum of La-Ce alloy. (b) SEM photo at position 2 (c) Upper: SEM photo at position 3, Middle: Ce distribution, Below: La distribution

Run #L1

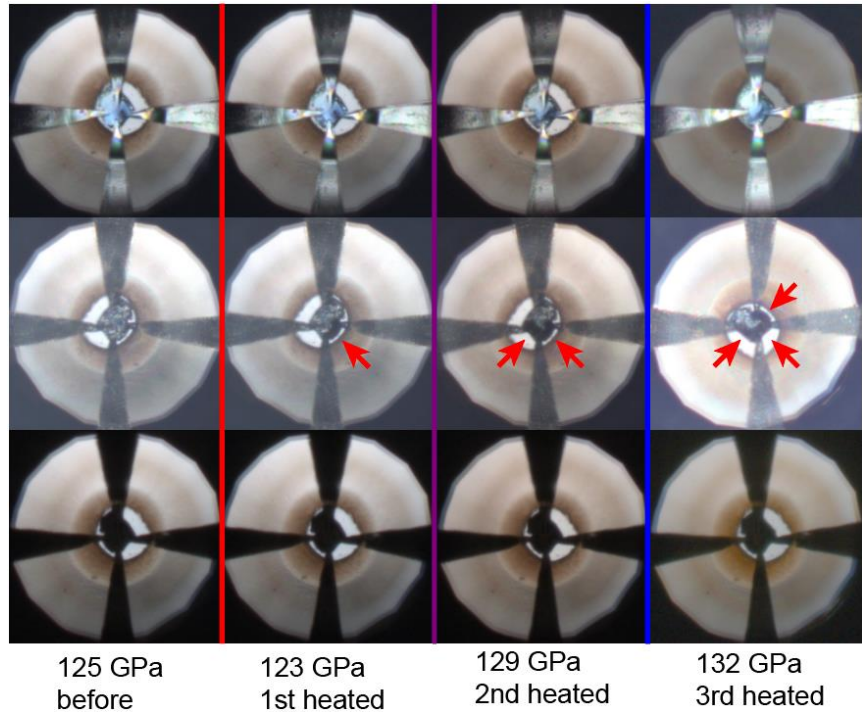


Fig. S15. Photographs of the sample in cell #L1 before and after laser heating for three times. The tips of four Pt electrodes were compressed to the edge of sample directly. The arrows point to the changes of sample after heating.

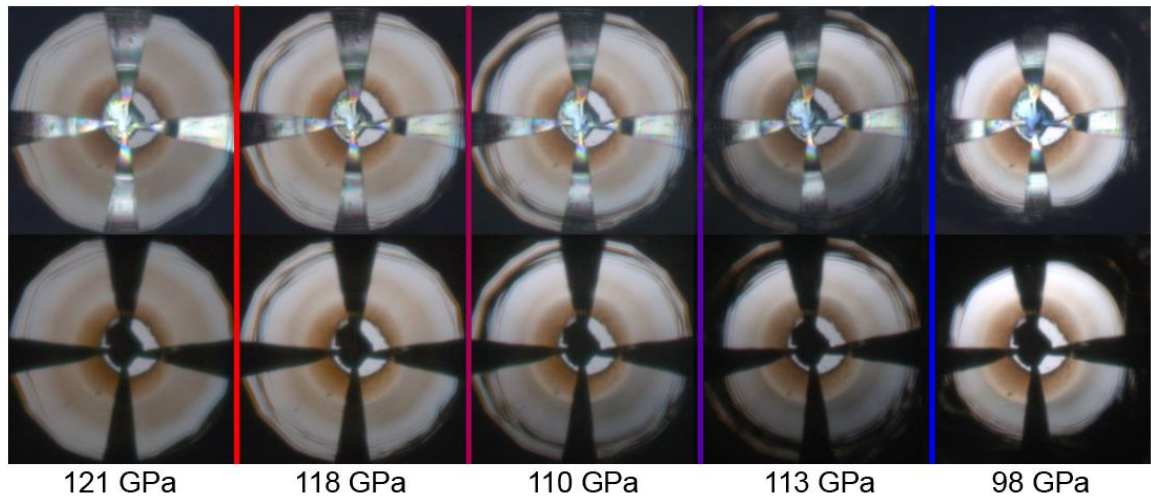


Fig. S16. Behavior of the diamond's bevel during decompression of cell #L1 from different photographic views.

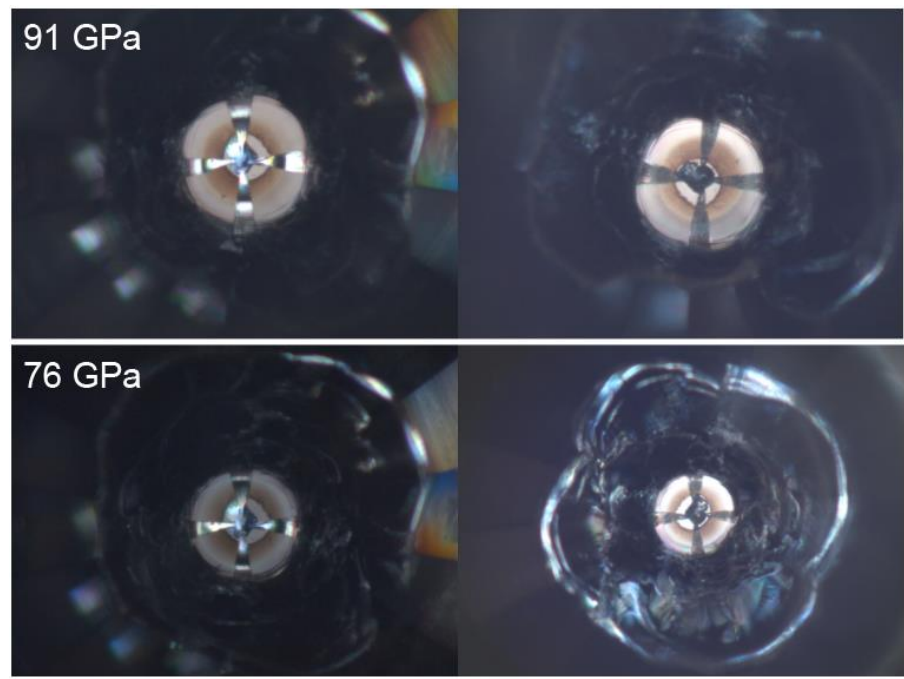


Fig. S17. Photographs of the diamonds of cell #L1 from both side at 91 GPa and 76 GPa.

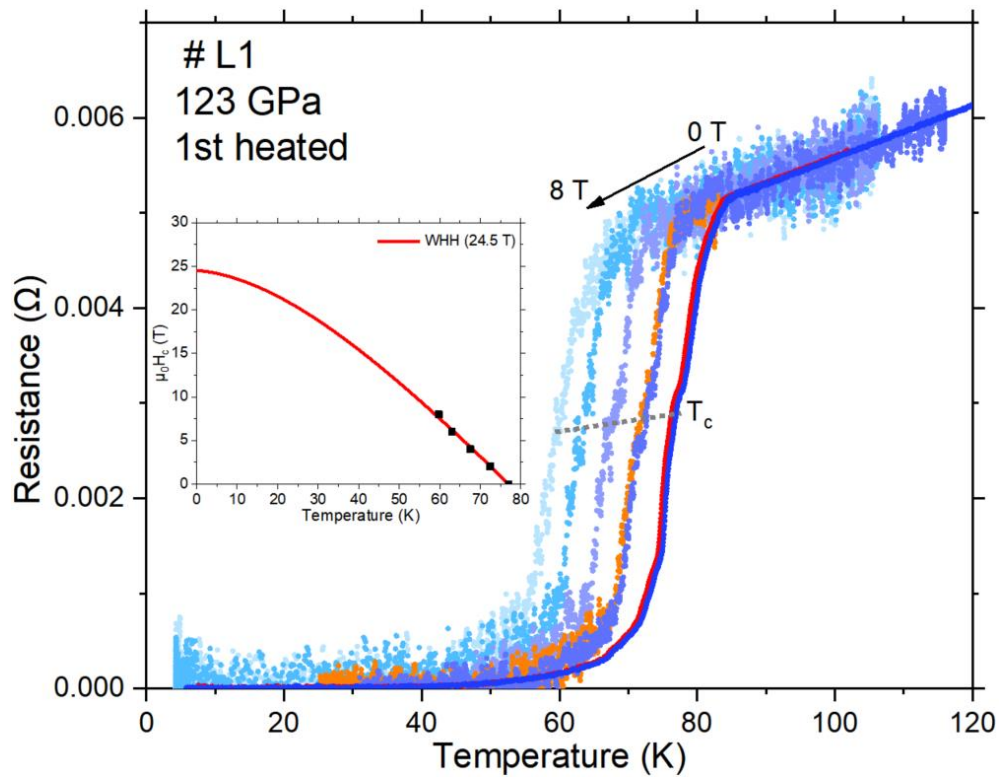


Fig. S18. Superconducting transition of #L1 characterized by the temperature dependence of resistance in the external magnetic field at 123 GPa after first laser heating. Inset is the WHH fitting of experimental data.

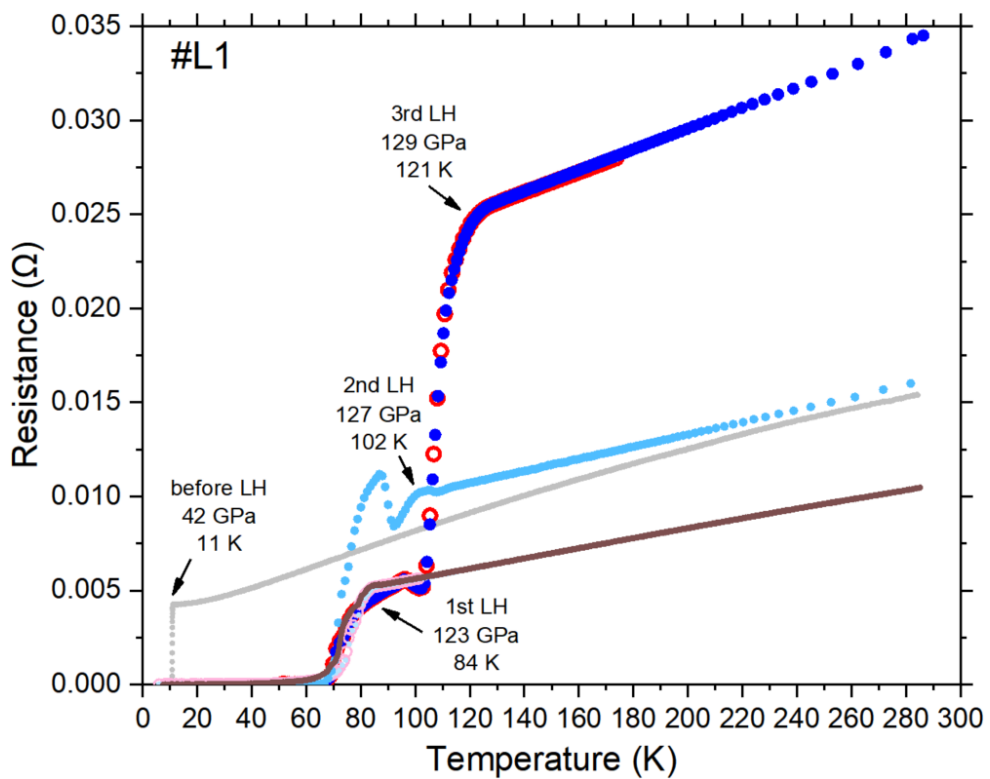


Fig. S19. Electrical resistance as a dependence of temperature after totally 3 times laser heating (LH). Solid circles represent the cooling cycle, and open circles represent the warming cycle. The horizontal density of data points indicates the rate of temperature.

Run #L2

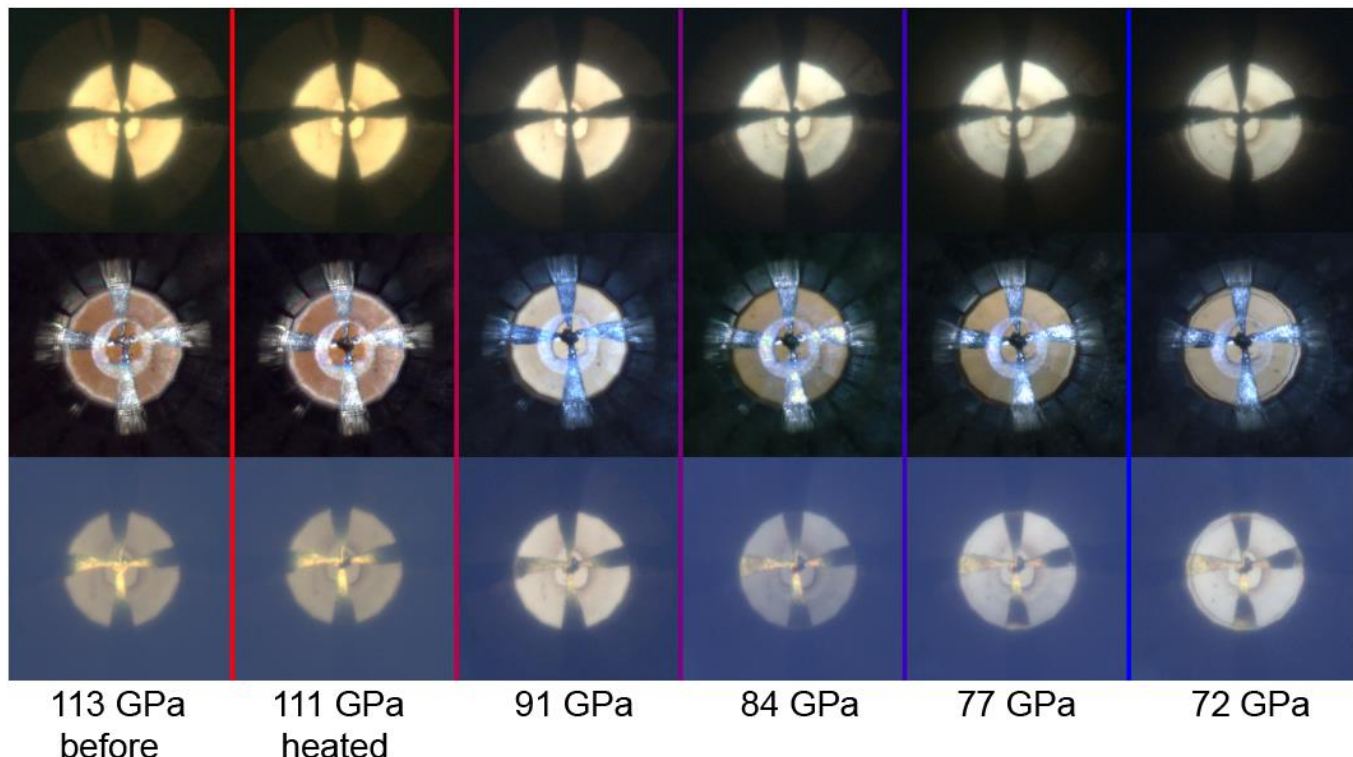


Fig. S20. Behavior of the diamond's bevel during decompression of cell #L2 from different photographic

views.

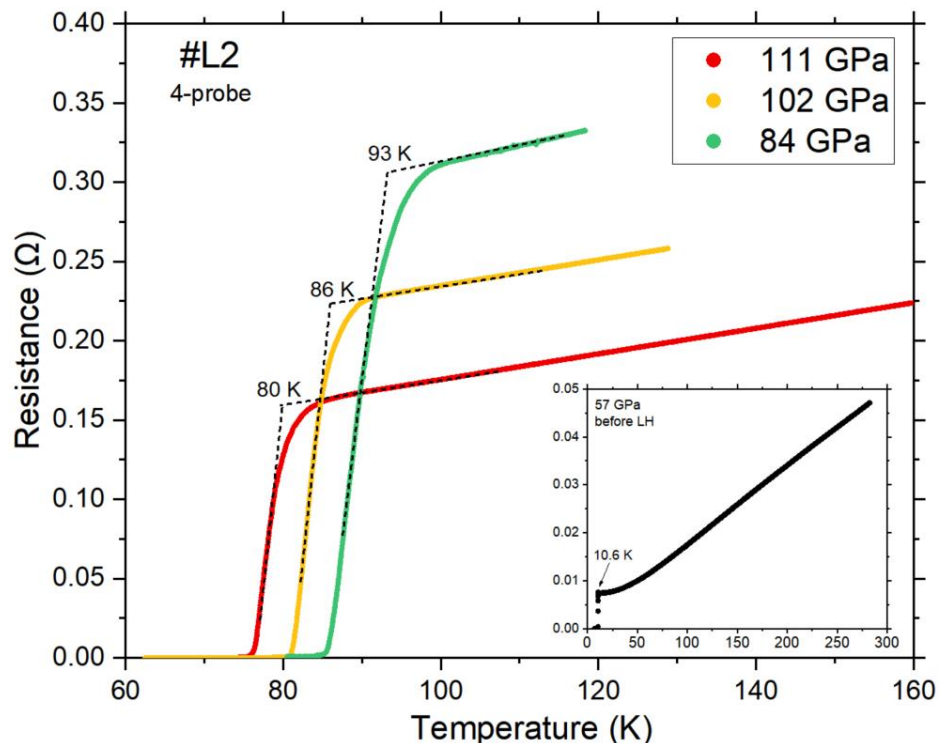


Fig. S21. Superconducting transition of LaH_x in cell #L2 characterized by 4-probe electrical resistance measurements as a dependence of temperature. Inset is the SC transition of pure La at 57 GPa before laser heating.

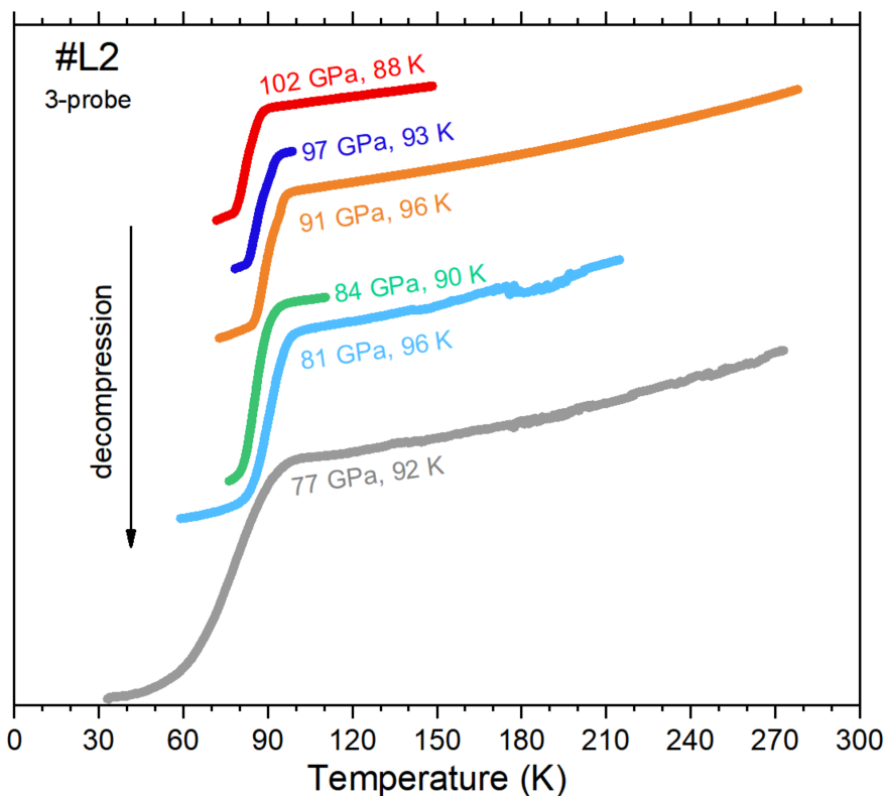


Fig. S22. Superconducting transition of LaH_x in cell #L2 characterized by 3-probe electrical resistance measurements as a dependence of temperature during decompression. The obtained curves are plotted in stack style.

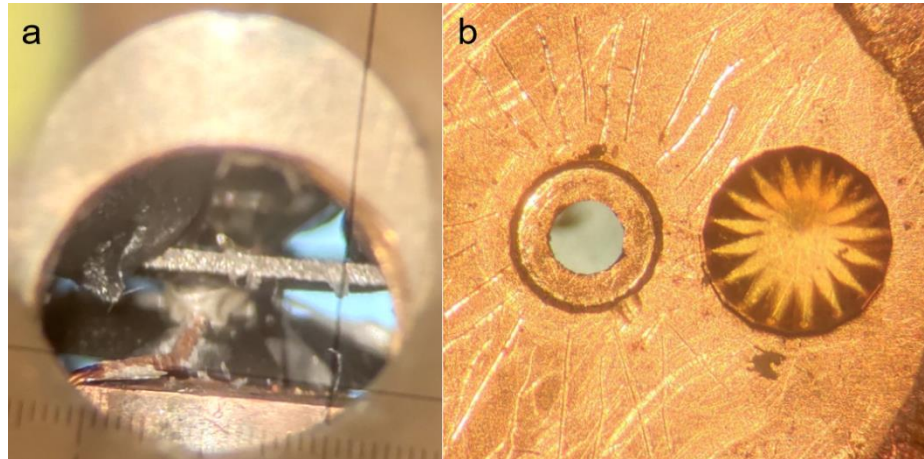


Fig. S23. (a) The photograph of dehiscent black resin of cell #L2. (b) Indentation on the BeCu block created by NPD diamond under high pressure. Divergence lines are artificial traces.

The NPD has a much smaller size and table than SCD which cause more serious squeeze to the block. Black resin suffers from the stress created by deformation and split at low temperature. Thus, one of the electrodes disconnected and reconnected occasionally. We measured the T_c using 4-probe (Fig. S21) and 3-probe (Fig. S23) methods alternately during decompression.

Run #L3

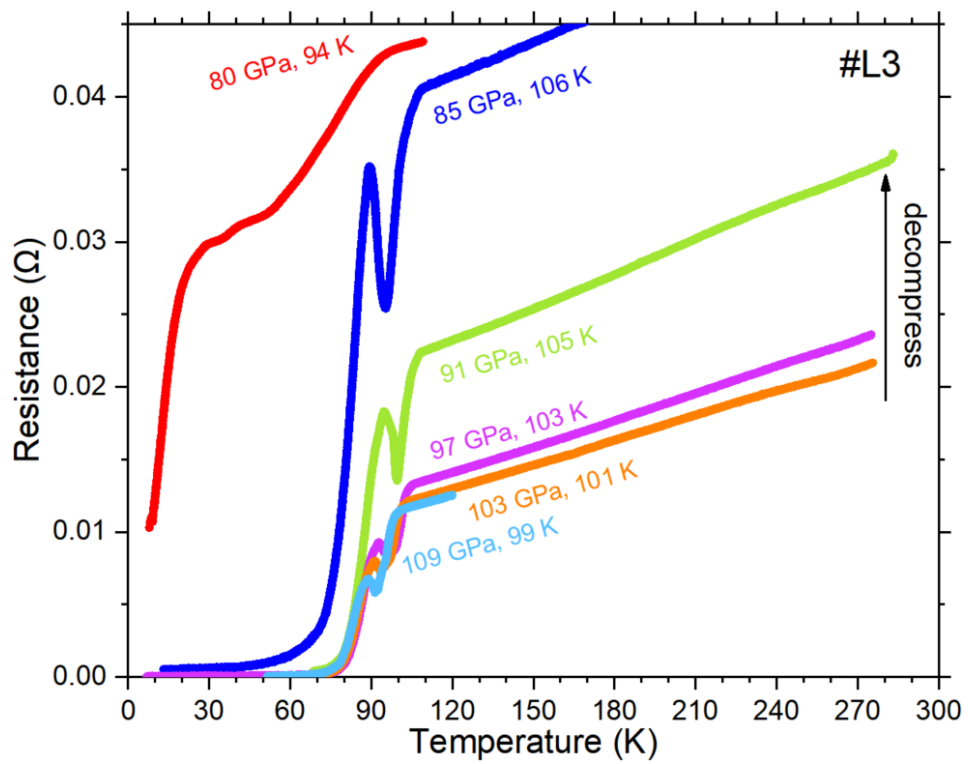


Fig. S24. Superconducting transition of the LaH_x in #L3 characterized by the temperature dependence of resistance.

Run #S

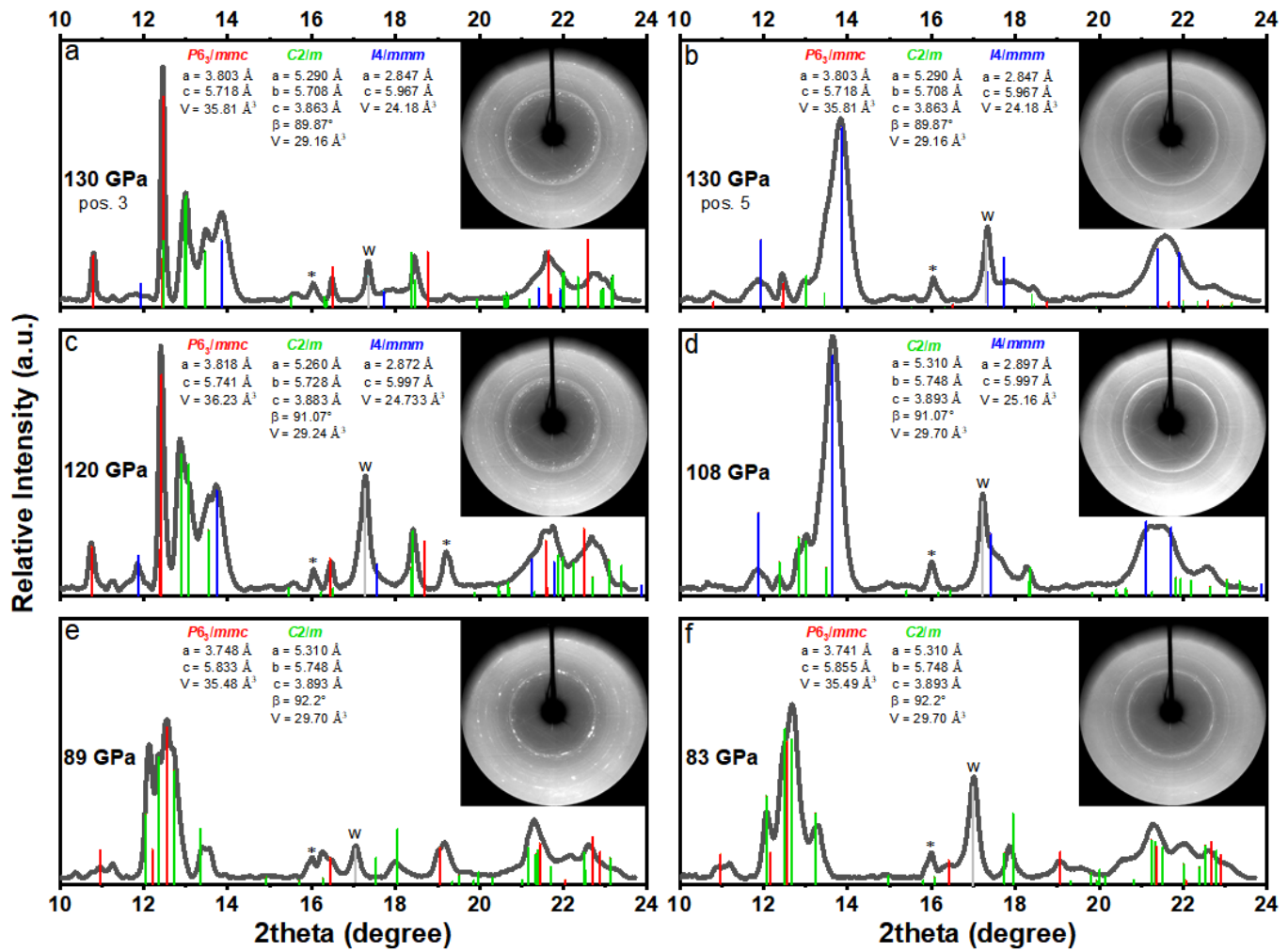


Fig. S25. Indexing of the synchrotron X-ray diffraction ($\lambda = 0.6199 \text{ \AA}$) data for cell #S during decompression.

Insets are the diffraction patterns.

References

[1] B. J. Baer, M. E. Chang, and W. J. Evans, Raman shift of stressed diamond anvils: Pressure calibration and culet geometry dependence, *J. Appl. Phys.* **104**, 034504 (2008).

- [2] Y. Akahama and H. Kawamura, Pressure calibration of diamond anvil Raman gauge to 310GPa, *J. Appl. Phys.* **100**, 043516 (2006).
- [3] C. Gao, Y. Han, Y. Ma, A. White, H. Liu, J. Luo, M. Li, C. He, A. Hao, X. Huang, Y. Pan, and G. Zou, Accurate measurements of high pressure resistivity in a diamond anvil cell, *Rev. Sci. Instrum.* **76**, 083912 (2005).
- [4] C. Prescher and V. B. Prakapenka, DIOPTAS: a program for reduction of two-dimensional X-ray diffraction data and data exploration, *High Press. Res.* **35**, 223 (2015).
- [5] V. Petříček, M. Dušek, and L. Palatinus, Crystallographic Computing System JANA2006: General features., *Z. Kristallogr. Cryst. Mater.* **229**, 345 (2014).
- [6] A. Le Bail, H. Duroy, and J. L. Fourquet, Ab-initio structure determination of LiSbWO₆ by X-ray powder diffraction, *Mater. Res. Bull.* **23**, 447 (1988).